arXiv:1010.4509v2 [hep-ph] 25 Oct 2010

Factorization and resummation of t-channel single top quark production

Jian Wang,[1] Chong Sheng Li*,[1,2] Hua Xing Zhu,[1] and Jia Jun Zhang[1,3]

[1]*Department of Physics and State Key Laboratory of Nuclear Physics and Technology,*
Peking University, Beijing, 100871, China

[2]*Center for High Energy Physics, Peking University, Beijing, 100871, China*

[3]*Nuclear Science Division, MS 70R0319,*
Lawrence Berkeley National Laboratory, Berkeley, CA 94720, USA

Abstract

We investigate the factorization and resummation of t-channel single top (antitop) quark production in the SM at both the Tevatron and the LHC in SCET. We find that the resummation effects decrease the NLO cross sections by about 3% at the Tevatron and about 2% at the LHC. And the resummation effects significantly reduce the factorization scale dependence of the total cross section. The transfer momentum cut dependence and other matching scale dependencies are also discussed. We also show that when our numerical results for s- and t-channel single top production at the Tevatron are combined, it is closer to the experimental result than the one reported in the previous literatures.

---

* Electronic address: csli@pku.edu.cn

I. INTRODUCTION

Top quark is an interesting particle in the standard model (SM) because of its large mass. It may play a special role in the electroweak symmetry breaking mechanism. Its properties such as mass [1], lifetime [2], spin, couplings to other particles and production mechanism deserve to be studied precisely.

The hadronic production of the single top production provides an important opportunity to study the charged weak current interactions of the top quark, e.g., the structure of the the Wtb vertex [3]. Besides, it is a background for many new physics processes. However, due to the difficulties to discriminate its signatures from the large background, it is only recently that D0 [4] and CDF [5] collaborations have observed the single top production at the Tevatron.

In the three main production modes of the top quark, the t-channel is specially important because of its largest cross section, which has been extremely studied, including the next-to-leading order (NLO) corrections in [6–12]. Their results show that the NLO corrections are about 5% and 9% at the LHC and Tevatron, respectively. Also, parton shower Monte Carlo simulation was considered in [13, 14]. Threshold resummation for this process was calculated in [15–17], where only large soft and collinear gluon corrections were resummed and the resummed cross section was expanded up to $\mathcal{O}(\alpha_s^3)$.

In this paper, we use the framework of soft-collinear effective theory (SCET) [18–22] to give a resummed cross section of t-channel single top production, which contains all contributions from large logarithms in hard, jet and soft functions to all orders. There is a strong motivation for performing this calculation because the hard functions of this process, compared with soft functions, is not small, but refs. [15–17] only resum the soft and jet effects to next-to-next-to-leading logarithmic (NNLL) order, using the traditional method, and leave the hard effects unresummed. In the SCET approach, the different scales in a process can be separated because the soft and collinear degrees can be decoupled by the redefinition of the fields. At each scale, we only need to deal with the relevant degrees of freedom. Their dependencies on the scale are controlled by the renormalization group (RG) equations, and the hard, jet and soft effects can be resummed conveniently.

This paper is organized as follows. In section II, we give the factorization and resummation formalism of this process in momentum space. In section III, each factor in the resummed cross section is calculated. In section IV, we present the numerical results for this process at the Tevatron and LHC, respectively. We conclude in section V.

II. FACTORIZATION AND RESUMMATION FORMALISM

Following the same factorization formalism as in our previous paper [23], the partonic differential cross section of t-channel can be written as

$$\frac{d\hat{\sigma}^{\rm thres}}{d\hat{t}d\hat{u}} = \sum_{ij} \frac{\lambda_{0,ij}}{64\pi N_c^2 \hat{s}^2} \int_0^{s_4/(2E_1)} dk^+ \, H_{IJ}(\mu) S_{JI}(k^+,\mu) J(s_4 - 2E_1 k^+,\mu), \tag{1}$$

with

$$\lambda_{0,ij} = \frac{e^4}{\sin^4\theta_W} |V_{ij}|^2 |V_{tb}|^2 \frac{(\hat{s}-m_t^2)\hat{s}}{(\hat{t}-M_W^2)^2}. \tag{2}$$

We use the same definitions of all above notations as [23] and also choose the independent singlet-octet basis in color space used in [23]. Because of the special color structure of this process at leading order (LO), the hard function matrix elements do not contribute to the cross section except for H_{11} at the NLO accuracy. In SCET, there is a RG evolution factor connecting the hard scale μ_h and the final common scale μ, which would contain contributions from non-diagonal elements in its anomalous dimension matrix. However, these contributions are so small, as we saw in ref. [23], that we can neglect them. Therefore, we can consider this channel as a double deep-inelastic-scattering (DDIS) process [8] and assume that the hard function H_{11} can be factorized into two parts, i.e. H_{up} and H_{dn}, which represent corrections from the up fermion line and down fermion line in the Feynman diagram 1, respectively. And eq. (1) can be simplified to

$$\frac{d\hat{\sigma}^{\rm thres}}{d\hat{t}d\hat{u}} = \sum_{ij} \frac{\lambda_{0,ij}}{64\pi N_c^2 \hat{s}^2} \int_0^{s_4/(2E_1)} dk^+ H_{up}(\mu) H_{dn}(\mu) J(s_4 - 2E_1 k^+,\mu) S(k^+,\mu). \tag{3}$$

III. THE HARD, JET AND SOFT FUNCTIONS AT NLO

At the NNLL accuracy, we need the explicit expressions of hard, jet and soft functions up to NLO in perturbation theory. In this section, we show the calculations of them.

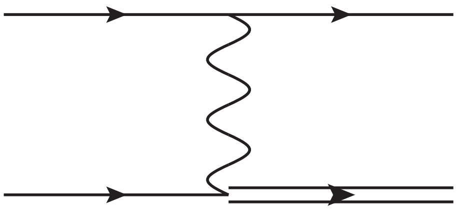

FIG. 1: The LO Feynman diagram of the t-channel single top production.

A. Hard functions

The hard functions are the absolute square of the Wilson coefficients of the operators, which can be obtained by matching the full theory onto SCET. In practice, we need to calculate the one-loop on-shell Feynman diagrams of this process in both the full theory and SCET. In dimensional regularization(DR), the facts that the IR structure of the full theory and the effective theory is identical and the on-shell integrals are scaleless and vanish in SCET imply that the IR divergence of the full theory is just the negative of the UV divergence of SCET. After calculating the one-loop on-shell Feynman diagrams, we get the hard functions at NLO are as follows:

$$H_{up}(\mu_{h,up}) = 1+\frac{C_F\alpha_s(\mu_{h,up})}{4\pi}\left(-2\ln^2\frac{-\hat{t}}{\mu_{h,up}^2}+6\ln\frac{-\hat{t}}{\mu_{h,up}^2}+c_1^{H,up}\right), \tag{4}$$

$$H_{dn}(\mu_{h,dn}) = 1+\frac{C_F\alpha_s(\mu_{h,dn})}{4\pi}\left(-4\ln^2\frac{-t+m_t^2}{\mu_{h,dn}m_t}+10\ln\frac{-t+m_t^2}{\mu_{h,dn}m_t}+c_1^{H,dn}\right), \tag{5}$$

with

$$c_1^{H,up} = -16+\frac{\pi^2}{3}, \tag{6}$$

$$\begin{aligned} c_1^{H,dn} &= -\frac{2}{\lambda}\ln(1-\lambda)+2\ln^2(1-\lambda)+6\ln(1-\lambda)+4\text{Li}_2(\lambda)-12-\frac{\pi^2}{6} \\ &\quad +\frac{2m_t^2\hat{u}}{\hat{t}(\hat{s}-m_t^2)}\ln\frac{m_t^2}{m_t^2-\hat{t}}, \end{aligned} \tag{7}$$

where $\lambda=\hat{t}/(\hat{t}-m_t^2)$. The hard functions have a well behaved expansion in powers of the coupling constant, if $\mu_{h,up}$ and $\mu_{h,dn}$ are taken to be of order the natural scales, $\mu_{h,up}\sim\sqrt{-\hat{t}}$ and $\mu_{h,dn}\sim(-\hat{t}+m_t^2)/m_t$, respectively. From eqs.(4, 5), we can write the RG equations of hard functions as

$$\frac{d}{d\ \ln\mu_{h,up}} H_{up}(\mu_{h,up}) \ = \ \left(2\Gamma_{\rm cusp}\ln\frac{-\hat{t}}{\mu^2_{h,up}} + 2\gamma^V_{up}\right) H_{up}(\mu_{h,up}), \tag{8}$$

$$\frac{d}{d\ \ln\mu_{h,dn}} H_{dn}(\mu_{h,dn}) \ = \ \left(2\Gamma_{\rm cusp}\ \ln\frac{-\hat{t}+m_t^2}{\mu_{h,dn}m_t} + 2\gamma^V_{dn}\right) H_{dn}(\mu_{h,dn}), \tag{9}$$

where $\Gamma_{\rm cusp}$ is related to the cusp anomalous dimension of Wilson loops with light-like segments [24], while γ^V_{up} and γ^V_{dn} accounts for single-logarithmic evolution. Their expressions are shown in appendix A.

After solving the RG equations, we get the hard functions at an arbitrary scale μ:

$$H_{up}(\mu) \ = \ \exp\left[4S(\mu_{h,up},\mu) - 2a^V_{up}(\mu_{h,up},\mu)\right]\left(\frac{-\hat{t}}{\mu^2_{h,up}}\right)^{-2a_\Gamma(\mu_{h,up},\mu)} H_{up}(\mu_{h,up}), \tag{10}$$

$$H_{dn}(\mu) \ = \ \exp\left[2S(\mu_{h,dn},\mu) - 2a^V_{dn}(\mu_{h,dn},\mu)\right]\left(\frac{-\hat{t}+m_t^2}{\mu_{h,dn}m_t}\right)^{-2a_\Gamma(\mu_{h,dn},\mu)} H_{dn}(\mu_{h,dn}), \tag{11}$$

where $S(\mu_{h,up},\mu)$ and a^V_{up} are defined as [25]

$$S(\mu_{h,up},\mu) \ = \ -\int_{\alpha_s(\mu_{h,up})}^{\alpha_s(\mu)} d\alpha \frac{\Gamma_{\rm cusp}(\alpha)}{\beta(\alpha)} \int_{\alpha_s(\mu_{h,up})}^{\alpha} \frac{d\alpha'}{\beta(\alpha')}, \tag{12}$$

$$a^V_{up}(\mu_{h,up},\mu) \ = \ -\int_{\alpha_s(\mu_{h,up})}^{\alpha_s(\mu)} d\alpha \frac{\gamma^V_{dn}(\alpha)}{\beta(\alpha)}, \tag{13}$$

and similarly for $S(\mu_{h,dn},\mu)$, a_Γ and a^V_{dn}.

B. Jet function

The jet function $J(p^2,\mu)$ is defined as [26]

$$\theta(p^0)p^- J(p^2,\mu) = \frac{1}{8\pi N_c}\int \frac{d^4p'}{(2\pi)^4} {\rm Tr}\langle 0|\bar{\chi}(-p')\bar{\not{n}}_1\chi(-p)|0\rangle. \tag{14}$$

The RG evolution of the jet function is given by [25]

$$\frac{dJ(p^2,\mu)}{d\ln\mu} = \left(-2\Gamma_{\rm cusp}\ln\frac{p^2}{\mu^2} - 2\gamma^J\right) J(p^2,\mu) + 2\Gamma_{\rm cusp}\int_0^{p^2} dq^2\, \frac{J(p^2,\mu) - J(q^2,\mu)}{p^2-q^2}. \tag{15}$$

To solve this integro-differential evolution equation, we use the Laplace transformed jet function:

$$\widetilde{j}(\ln\frac{Q^2}{\mu^2},\mu) = \int_0^\infty dp^2\ \exp(-\frac{p^2}{Q^2 e^{\gamma_E}}) J(p^2,\mu), \tag{16}$$

which satisfies the the RG equation

$$\frac{d}{d\ln\mu}\widetilde{j}(\ln\frac{Q^2}{\mu^2},\mu)=\left(-2\Gamma_{\text{cusp}}\ln\frac{Q^2}{\mu^2}-2\gamma^J\right)\widetilde{j}(\ln\frac{Q^2}{\mu^2},\mu). \tag{17}$$

Then the jet function at an arbitrary scale μ is given by

$$J(p^2,\mu)=\exp\left[-4S(\mu_j,\mu)+2a^J(\mu_j,\mu)\right]\widetilde{j}(\partial_{\eta_j},\mu_j)\frac{1}{p^2}\left(\frac{p^2}{\mu_j^2}\right)^{\eta_j}\frac{e^{-\gamma_E\eta_j}}{\Gamma(\eta_j)}, \tag{18}$$

where $\eta_j=2a_\Gamma(\mu_j,\mu)$. The Laplace transformed jet function $\widetilde{j}(L,\mu)$ at NLO is

$$\widetilde{j}(L,\mu)\;=\;1+\frac{\alpha_s}{4\pi}\left\{\frac{\Gamma_0^2}{2}L^2+\gamma_0^J L+c_1^J\right\}, \tag{19}$$

where $c_1^J=\left(7-\frac{2}{3}\pi^2\right)C_F$.

C. Soft function

The soft function $S(k^+,\mu)$, which describe soft interactions between all colored particles, is defined as [26]

$$S(k^+,\mu)\;=\;\frac{1}{N_c^2}\int dk^+\frac{d^4k_s'}{(2\pi)^4}\frac{d^4k_s}{(2\pi)^4}\langle 0|\mathcal{O}_S^{\dagger,fedc}(k_s')\delta[k^+-n_1\cdot k_s]\mathcal{O}_S^{cdef}(k_s)|0\rangle, \tag{20}$$

where

$$\mathcal{O}_S^{cdef}(k_s)\;=\;\int d^4x e^{-ik_s\cdot x}\mathbf{T}\left[\left(Y_{n_b}^\dagger(x)Y_{n_a}(x)\right)^{cd}\left((\tilde{Y}_{v_2}^\dagger(x)\tilde{Y}_{n_1}(x)\right)^{ef}\right]. \tag{21}$$

Here $\mathbf{T}$ is the time-ordering operator required to ensure the proper ordering of soft gluon fields in the soft Wilson line [27], which is defined as

$$Y_n(x)=\mathbf{P}\exp\left(ig_s\int_{-\infty}^0 ds\,n\cdot A_s^a(x+sn)t^a\right) \tag{22}$$

for incoming Wilson lines, and

$$\tilde{Y}_n(x)=\mathbf{P}\exp\left(-ig_s\int_0^\infty ds\,n\cdot A_s^a(x+sn)t^a\right) \tag{23}$$

for out going Wilson lines, respectively.

The soft function can be calculated in SCET or in the full theory in the Eikonal approximation [28]. In DR, actually, we only need to calculate the non-vanishing real emission diagrams, as shown in figure 2, which give

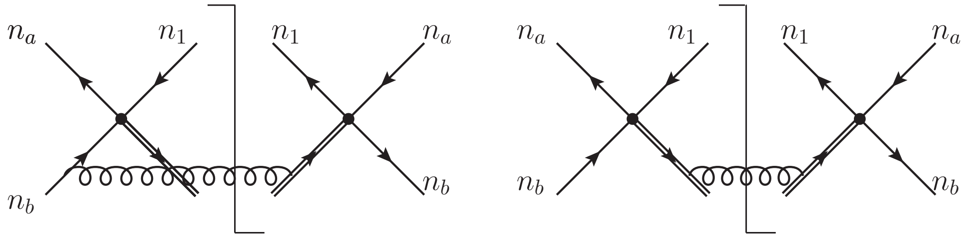

FIG. 2: Non-vanishing diagrams contributing to the soft function at NLO. The contribution from the left and right diagrams are denoted as S_{bt} and S_{tt}, respectively.

$$\begin{aligned} S^{(1)}_{bt}(k,\mu) \;=\; & \frac{2g_s^2 C_F \mu^{2\epsilon}}{(2\pi)^{d-1}}\frac{1}{2}\int_0^\infty \mathrm{d}q^+ \int_0^\infty \mathrm{d}q^- \int \mathrm{d}^{d-2}q_\perp \\ & \delta(q^+q^- - q_\perp^2)\delta(k - n_1\cdot q)\frac{n_b\cdot v}{(q\cdot n_b)(q\cdot v)}, \end{aligned} \tag{24}$$

and

$$\begin{aligned} S^{(1)}_{tt}(k,\mu) \;=\; & \frac{-g_s^2 C_F \mu^{2\epsilon}}{(2\pi)^{d-1}}\frac{1}{2}\int_0^\infty \mathrm{d}q^+ \int_0^\infty \mathrm{d}q^- \int \mathrm{d}^{d-2}q_\perp \\ & \delta(q^+q^- - q_\perp^2)\delta(k - n_1\cdot q)\frac{1}{(q\cdot v)^2}, \end{aligned} \tag{25}$$

respectively. Evaluating these integrals, we get

$$S_{bt}(k,\mu) \;=\; \delta(k) + \frac{2C_F\alpha_s}{4\pi}\left\{4\left[\frac{\ln\frac{k}{\tilde{\mu}}}{k}\right]_\star^{[k,\tilde{\mu}]} + \delta(k)c^S_{bt}\right\}, \tag{26}$$

and

$$S_{tt}(k,\mu) \;=\; \delta(k) - \frac{C_F\alpha_s}{4\pi}\left\{4\left[\frac{1}{k}\right]_\star^{[k,\tilde{\mu}]} + \delta(k)c^S_{tt}\right\}, \tag{27}$$

respectively, where $\tilde{\mu} = \mu/\sqrt{(2n_{b\bar{b}})/n_1^{+2}} = (\mu(-\hat{u})m_t)/(2(-\hat{t}+m_t^2)E_1)$. The explicit expressions of c^S_{bt} and c^S_{tt} are given in appendix B. And the soft function $S(k,\mu) = S_{bt}(k,\mu) + S_{bt}(k,\mu)$, similar to the jet function, satisfies the RG equation

$$\frac{d}{d\ln\mu}S(k,\mu) = \left[-2\Gamma_{\text{cusp}}\ln\frac{k}{\tilde{\mu}} + 2\gamma^S\right]S(k,\mu) + 2\Gamma_{\text{cusp}}\int_0^k dk'\frac{S(k,\mu)-S(k',\mu)}{k-k'}. \tag{28}$$

The solution to this equation is

$$S(k,\mu) = \exp\bigl[-2S(\mu_s,\mu) - 2a^S(\mu_s,\mu)\bigr]\widetilde{s}(\partial_{\eta_s},\mu_s)\frac{1}{k}\left(\frac{k}{\tilde{\mu}_s}\right)^{\eta_s}\frac{e^{-\gamma_E\eta_s}}{\Gamma(\eta_s)}, \tag{29}$$

where $\eta_s = 2a_\Gamma(\mu_s,\mu)$. The Laplace transformed soft function $\widetilde{s}(L,\mu)$ at NLO is given by

$$\widetilde{s}(L,\mu) \;=\; 1 + \frac{\alpha_s}{4\pi}\left\{\Gamma_0 L^2 - 2\gamma_0^S L + c_1^S\right\}, \tag{30}$$

where $c_1^S = (2c^S_{bt} - c^S_{tt} + \frac{2\pi^2}{3})C_F$.

D. Final resummed differential cross section

After combining the hard, jet and soft function together, according to eq. (3), we obtain the resummed differential cross section for t-channel single top production

$$\begin{aligned}
\frac{d\hat{\sigma}^{\text{thres}}}{d\hat{t}d\hat{u}} = & \sum_{ij} \frac{\lambda_{0,ij}}{64\pi N_c^2 \hat{s}^2} \\
& \exp\left[4S(\mu_{h,up},\mu_{F,up}) - 2a_{up}^V(\mu_{h,up},\mu_{F,up})\right] \left(\frac{-\hat{t}}{\mu_{h,up}^2}\right)^{-2a_\Gamma(\mu_{h,up},\mu_{F,up})} H_{up}(\mu_{h,up}) \\
& \exp\left[2S(\mu_{h,dn},\mu_{F,dn}) - 2a_{dn}^V(\mu_{h,dn},\mu_{F,dn})\right] \left(\frac{-\hat{t}+m_t^2}{\mu_{h,dn} m_t}\right)^{-2a_\Gamma(\mu_{h,dn},\mu_{F,dn})} H_{dn}(\mu_{h,dn}) \\
& \exp\left[-4S(\mu_j,\mu_{F,up}) + 2a^J(\mu_j,\mu_{F,up})\right] \left(\frac{m_t^2}{\mu_j^2}\right)^{\eta_j} \\
& \exp\left[-2S(\mu_s,\mu_{F,dn}) - 2a^S(\mu_s,\mu_{F,dn})\right] \left(\frac{m_t(-\hat{t}+m_t^2)}{\mu_s(-\hat{u})}\right)^{\eta_s} \\
& \widetilde{j}(\partial_\eta + L_j,\mu_j)\widetilde{s}(\partial_\eta + L_s,\mu_s)\frac{1}{s_4}\left(\frac{s_4}{m_t^2}\right)^{\eta} \frac{e^{-\gamma_E \eta}}{\Gamma(\eta)},
\end{aligned} \tag{31}$$

where $\eta = \eta_j + \eta_s$ and $L_j = \ln(m_t^2/\mu_j^2), L_s = \ln(m_t(-\hat{t}+m_t^2))/(\mu_s(-\hat{u}))$. In the above expression, we have chosen $\mu = \mu_{F,up}$ or $\mu = \mu_{F,dn}$ to avoid the evolution of the parton distribution functions.

If we set scales $\mu_{h,up}$, $\mu_{h,dn}$, μ_j, μ_s equal to the common scale μ, which is conveniently chosen as the factorization scale $\mu_{F,up} = \mu_{F,dn} = \mu_F$, then we recover the threshold singular plus distributions, which should appear in the fixed-order calculation. Up to order α_s^2, we have

$$
\begin{aligned}
\frac{\lambda_{0,ij}}{64\pi N_c^2\hat{s}^2}\frac{d\hat{\sigma}_{ij}^{\rm thres}}{d\hat{t}d\hat{u}} =\ & \delta(s_4)+\frac{\alpha_s}{4\pi}\Bigg\{3\Gamma_0\Bigg[\frac{\ln(s_4/m_t^2)}{s_4}\Bigg]_+ + \big[\gamma_0^J-2\gamma_0^S+(L_j+2L_s)\Gamma_0\big]\Bigg[\frac{1}{s_4}\Bigg]_+\Bigg\} \\
&+\left(\frac{\alpha_s}{4\pi}\right)^2\Bigg\{\frac{9\Gamma_0^2}{2}\Bigg[\frac{\ln^3(s_4/m_t^2)}{s_4}\Bigg]_+ +\big[\frac{9}{2}(L_j+2L_s)\Gamma_0^2-\frac{1}{2}(5\beta_0-9\gamma_0^J-18\gamma_0^S)\Gamma_0\big]\Bigg[\frac{\ln^2(s_4/m_t^2)}{s_4}\Bigg]_+ \\
&+\big[\frac{5\Gamma_0^2}{2}L_j^2+(4L_s\Gamma_0^2+(5\gamma_0^J-4\gamma_0^S-\beta_0)\Gamma_0)L_j+7\Gamma_0^2L_s^2+(4\gamma_0^J-14\gamma_0^S-4\beta_0)L_s-\frac{9\pi^2}{4}\Gamma_0^2 \\
&+3(c_1^H+c_1^J+c_1^S)\Gamma_0+(\gamma_0^J-2\gamma_0^S)^2-\beta_0(\gamma_0^J-4\gamma_0^S)+3\Gamma_1\big]\Bigg[\frac{\ln(s_4/m_t^2)}{s_4}\Bigg]_+ +\big[\frac{\Gamma_0^2}{2}L_j^3+\{L_s\Gamma_0^2 \\
&+\frac{1}{2}(3\gamma_0^J-2\gamma_0^S-\beta_0)\Gamma_0\}L_j^2+\{\Gamma_0^2L_s^2+2(\gamma_0^J-\gamma_0^S)\Gamma_0L_s+(c_1^J+c_1^S)\Gamma_0+(\gamma_0^J-2\gamma_0^S-\beta_0)\gamma_0^J \\
&-\frac{3\pi^2}{4}\Gamma_0^2+\Gamma_1\}L_j+2\Gamma_0^2L_s^3+(\gamma_0^J-6\gamma_0^S-2\beta_0)\Gamma_0L_s^2+\{-\frac{3\pi^2}{2}\Gamma_0^2+2(c_1^J+c_1^S)\Gamma_0 \\
&+2(2\gamma_0^S-\gamma_0^J+2\beta_0)\gamma_0^S+2\Gamma_1\}L_s+9\zeta_3\Gamma_0^2-(\frac{3\gamma_0^J}{4}-\frac{3\gamma_0^S}{2}-\frac{5\beta_0}{12})\pi^2\Gamma_0+(\gamma_0^J-2\gamma_0^S-\beta_0)c_1^J \\
&+(\gamma_0^J-2\gamma_0^S-2\beta_0)c_1^S+\gamma_1^J-2\gamma_1^S+\big\{\gamma_0^J-2\gamma_0^S+(L_j+2L_s)\Gamma_0\big\}c_1^H\big]\Bigg[\frac{1}{s_4}\Bigg]_+\Bigg\},
\end{aligned}
\tag{32}
$$

where $c_1^H=c_1^{H,up}+c_1^{H,dn}$. We find that all $\mathcal{O}(\alpha_s)$ and two front $\mathcal{O}(\alpha_s^2)$ singular plus distribution terms coincide with Kidonakis' [15].

Including the remaining terms in the NLO result which we do not resum, we obtain the final resummed differential cross section

$$
\begin{aligned}
\frac{d\hat{\sigma}^{\rm RES}}{d\hat{t}d\hat{u}} =\ & \frac{d\hat{\sigma}^{\rm thres}}{d\hat{t}d\hat{u}}\Big|_{\mu_{F,up},\mu_{F,dn},\mu_{h,up},\mu_{h,dn},\mu_j,\mu_s} \\
&+\frac{d\hat{\sigma}^{\rm NLO}}{d\hat{t}d\hat{u}}\Big|_{\mu_{F,up},\mu_{F,dn}}-\frac{d\hat{\sigma}^{\rm thres}}{d\hat{t}d\hat{u}}\Big|_{\mu_{F,up}=\mu_{F,dn}=\mu_{h,up}=\mu_{h,dn}=\mu_j=\mu_s}.
\end{aligned}
\tag{33}
$$

IV. NUMERICAL DISCUSSION

In this section, we discuss the numerical results of threshold resummation in t-channel single top production via SCET. In our calculation, there are four scales, except the two factorization scales, $\mu_{h,up},\mu_{h,dn},\mu_j,\mu_s$ explicitly, which are all arbitrary in principle and our final results should not depend on them. However, because the Wilson coefficients in each matching, expressed as hard, jet and soft functions, respectively, and the anomalous dimensions are evaluated in fixed-order perturbation theory, there are residual dependence on these scales. To illustrate the reliability of our evaluation, first, we investigate these scale uncertainties. In the discussion below, we focus on the scenario at the Tevatron and give a

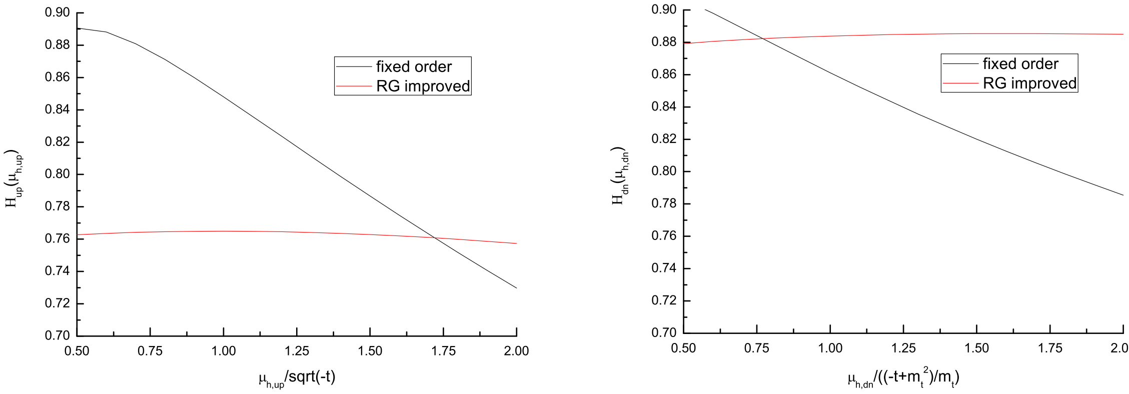

FIG. 3: The variations of $H_{up}(\mu_{h,up})$ and $H_{dn}(\mu_{h,dn})$ with $\mu_{h,up}$ and $\mu_{h,dn}$, respectively.

cut to $\sqrt{-\hat{t}}$[1], which is the transfer momentum of this process, because, based on the view point of effective theory, only processes of large transfer momentum are considered as hard processes with which we are concerned.

A. Scale choices and uncertainties

First, we discuss the dependence of $H_{up}(\mu_{h,up})$ on $\mu_{h,up}$. From eq.(4), in order to avoid large logarithms, we choose $\sqrt{-\hat{t}}$ as our natural hard(up) scale. The left curves in figure 3 illustrate the RG effects reduce the dependence of $H_{up}(\mu_{h,up})$ on $\mu_{h,up}$. And the correction induced by the RG-improved $H_{up}(\mu_{h,up})$ to the LO cross section is about -24%, which is significant. The right curves in figure 3 show the RG effects reduce the dependence of $H_{dn}(\mu_{h,dn})$ on $\mu_{h,dn}$, where we choose $(-\hat{t}+m_t^2)/m_t$ as our natural hard(down) scale. From these curves, we can see that the scale dependence is reduced and its RG-improved correction to LO cross section is about -11%.

Then, we examine the dependence of jet function on μ_j. Unlike the case of hard functions, because we perform the integration convoluting the jet and soft functions analytically, we can only choose the natural jet scale through the numerical results. In figure 4, we show that the natural jet scale is about 60 GeV around which the contribution of the fixed order jet function is minimal. Besides, the RG-improved jet function vary slowly, which indicates that

---

[1] For s-channel processes, the invariant mass of final state particles provides a natural cut to the transfer momentum $\sqrt{\hat{s}}$.

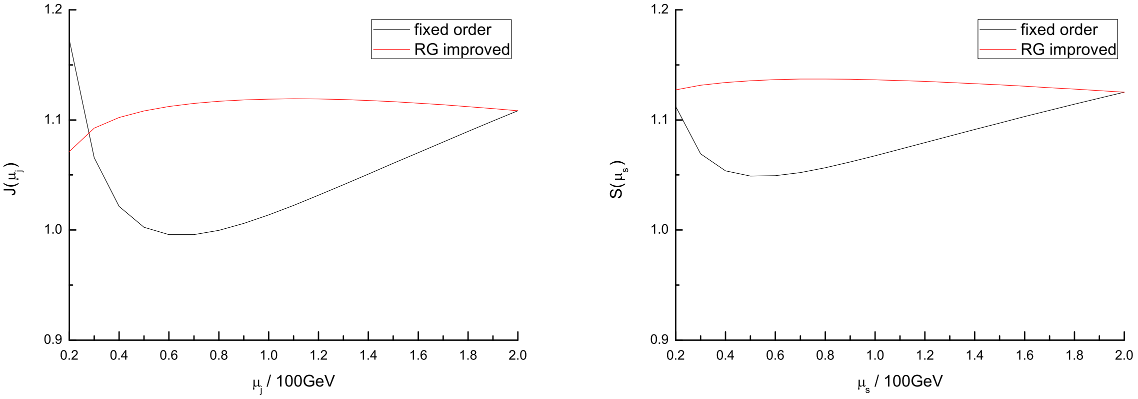

FIG. 4: The variations of $J(\mu_j)$ and $S(\mu_s)$ with μ_j and μ_s, respectively.

the scale dependence is significantly reduced. The correction induced by the RG-improved jet function to the LO cross section is about +12%.

The same case happens in the soft function. In principle, we may consider $2E_1k(-\hat{t}+m_t^2)/(-\hat{u})/m_t$ as the natural soft scale. But, in practice, from the numerical results in figure 4, we set the natural soft scale at 50 GeV, and find that the correction induced by the RG-improved soft function to the LO cross section is about +14%.

B. Resummed cross sections

We have chosen all the natural scales needed in this process. Now we give the numerical results of the resummed cross section. When discussing each scale dependence, we fixed the other scales at the natural scales chosen in the last subsection.

	$\mu_{F,up}$	$\mu_{F,dn}$	$\mu_{F,up}$ & $\mu_{F,dn}$
$\sigma_{\rm LO}$(pb)	$0.959^{+0.064}_{-0.055}$	$0.959^{-0.058}_{+0.041}$	$0.959^{-0.001}_{+0.016}$
$\sigma_{\rm NLO}$(pb)	$0.977^{+0.006}_{-0.004}$	$0.977^{-0.032}_{+0.021}$	$0.977^{-0.030}_{+0.026}$
$\sigma_{\rm RES}$(pb)	$0.948^{+0.047}_{-0.033}$	$0.948^{-0.041}_{+0.030}$	$0.948^{-0.012}_{+0.006}$

TABLE I: The variations of the resummed cross section and fixed order cross section with factorization scales at the Tevatron with $\sqrt{S}$=1.96 TeV, choosing $m_t = 175$ GeV and transfer momentum cut $\sqrt{-\hat{t}} > 80$ GeV.

In table I, we vary the factorization scales over the ranges 100 GeV $< \mu_{F,up}, \mu_{F,dn} <$

400 GeV. And table I shows that the resummation effects decrease the NLO cross section by about 3%. This is reasonable because we have seen above that the virtual effects are negative, and their absolute values are larger than those of jet and soft effects. These effects, when resummed to all order, would contribute large negative corrections which even overwhelm the positive jet and soft contributions. As a result, the resummed cross section is less than the LO order if the same parton distribution functions are applied, just as we did in this work. From table I we also can see the factorization scale dependence of resummed cross sections is reduced when the two factorization scales vary simultaneously, compared with NLO cross sections. But, if the factorization scales vary separately, the scale dependence get worse, thought still better than that of LO cross sections.

In table II, we show scale dependencies of the resummed cross section, where the scales vary over the ranges $\sqrt{-\hat{t}}/2 < \mu_{h,up} < 2\sqrt{-\hat{t}}$, $(-\hat{t}+m_t^2)/m_t/2 < \mu_{h,dn} < 2(-\hat{t}+m_t^2)/m_t$, 30 GeV $< \mu_j <$ 120 GeV and 25 GeV $< \mu_s <$ 100 GeV. And we can see that their uncertainties are all very small.

	$\mu_{h,up}$	$\mu_{h,dn}$	μ_j	μ_s
$\sigma_{\rm RES}$(pb)	$0.948^{+0.001}_{-0.010}$	$0.948^{-0.001}_{+0.005}$	$0.948^{-0.003}_{+0.009}$	$0.948^{-0.001}_{+0.005}$

TABLE II: The $\mu_{h,up}$, $\mu_{h,dn}$, μ_j and μ_s scale dependencies of resummed cross section at the Tevatron with $\sqrt{S}$=1.96 TeV, taking $m_t = 175$ GeV and transfer momentum cut $\sqrt{-\hat{t}} > 80$ GeV.

In table III, we show how the value of m_t affects our results. When the value of m_t varies from 171 GeV to 175 GeV, the resummed cross sections vary by about 6%.

m_t(GeV)	171	172	173	174	175
$\sigma_{\rm LO}$(pb)	1.032	1.013	0.995	0.977	0.959
$\sigma_{\rm NLO}$(pb)	1.037	1.026	1.010	0.987	0.977
$\sigma_{\rm RES}$(pb)	1.008	0.997	0.982	0.959	0.948

TABLE III: The m_t dependence of resummed cross section at the Tevatron with $\sqrt{S}$=1.96 TeV, taking transfer momentum cut $\sqrt{-\hat{t}} > 80$ GeV.

Table IV gives the transfer momentum cut dependence of the cross sections. It shows that the resummed cross section gets smaller when the transfer momentum cut is decreased since choosing a smaller transfer momentum cut means that more hard effects are resummed.

But as mentioned above, the transfer momentum cut can not be chosen too small for a hard process. Therefore, we choose 80 GeV as the natural transfer momentum cut in the numerical calculations.

$\sqrt{-\hat{t}}$(GeV)	> 60	> 70	> 80	> 90	> 100
$\sigma_{\rm RES}$(pb)	0.920	0.936	0.948	0.957	0.964

TABLE IV: The transfer momentum cut dependence of resummed cross section at the Tevatron with $\sqrt{S}$=1.96 TeV, taking $m_t = 175$ GeV.

In tables V, VI, VII, VIII, IX, and X, we present the results for the single top (antitop) production at the LHC for different top quark mass with $\sqrt{S} = 7, 10, \text{and } 14$ TeV, respectively. We can see that the resummation effects decrease the NLO cross sections by about 2% when the transfer momentum cut is chosen as 80 GeV. And the factorization scale dependencies of the cross section are reduced also.

C. Combined s and t channel cross sections

Table XI shows the combined numerical results for s- [23] and t-channel single top production at the Tevatron. From table XI, we see that our result is closer to the experimental result [29] than the one reported in the previous literatures[15–17].

V. CONCLUSION

We have studied the factorization and resummation of t-channel single top (antitop) quark production in the Standard Model at both the Tevatron and the LHC with SCET. Our results show that the resummation effects decrease the NLO cross sections by about 3% at the Tevatron and about 2% at the LHC, respectively. And the resummation effects significantly reduce the factorization scale dependence of the total cross section when the two factorization scales vary simultaneously, compared with the NLO results. We also show that when our numerical results for s- [23] and t-channel single top production at the Tevatron are combined, it is closer to the experimental result [29] than the one reported in the previous literatures[15–17] .

m_t(GeV)	171	172	173	174	175
$\sigma_{\rm LO}$(pb)	$44.9^{-3.1}_{+2.2}$	$44.4^{-3.1}_{+2.1}$	$43.9^{-3.0}_{+2.1}$	$43.5^{-3.0}_{+2.1}$	$43.0^{-2.9}_{+2.0}$
$\sigma_{\rm NLO}$(pb)	$42.6^{-0.8}_{+1.0}$	$42.2^{-0.7}_{+1.2}$	$41.9^{-0.6}_{+0.9}$	$41.6^{-0.8}_{+0.8}$	$41.1^{-0.7}_{+0.9}$
$\sigma_{\rm RES}$(pb)	$41.7^{-0.1}_{+0.2}$	$41.3^{-0.1}_{+0.3}$	$40.9^{-0.1}_{+0.1}$	$40.7^{-0.1}_{+0.1}$	$40.2^{-0.1}_{+0.1}$

TABLE V: The cross sections for t-channel single top production at LHC with $\sqrt{S}$=7 TeV, choosing transfer momentum cut $\sqrt{-\hat{t}} > 80$ GeV. The factorization scale uncertainties are also shown.

m_t(GeV)	171	172	173	174	175
$\sigma_{\rm LO}$(pb)	$90.9^{-7.7}_{+5.9}$	$90.0^{-7.6}_{+5.8}$	$89.2^{-7.5}_{+5.7}$	$88.4^{-7.4}_{+5.6}$	$87.5^{-7.4}_{+5.5}$
$\sigma_{\rm NLO}$(pb)	$86.1^{-1.9}_{+2.1}$	$85.5^{-1.9}_{+1.5}$	$84.6^{-1.5}_{+1.8}$	$83.3^{-0.8}_{+2.5}$	$83.0^{-1.2}_{+1.6}$
$\sigma_{\rm RES}$(pb)	$84.4^{-0.5}_{+0.4}$	$83.8^{-0.6}_{+0.1}$	$82.9^{-0.1}_{+0.2}$	$81.6^{-0.1}_{+0.8}$	$81.3^{-0.1}_{+0.6}$

TABLE VI: The cross sections for t-channel single top production at LHC with $\sqrt{S}$=10 TeV, choosing transfer momentum cut $\sqrt{-\hat{t}} > 80$ GeV. The factorization scale uncertainties are also shown.

m_t(GeV)	171	172	173	174	175
$\sigma_{\rm LO}$(pb)	$167.0^{-16.5}_{+13.2}$	$165.6^{-16.3}_{+13.0}$	$164.2^{-16.1}_{+12.9}$	$162.7^{-16.0}_{+12.7}$	$161.3^{-15.8}_{+12.8}$
$\sigma_{\rm NLO}$(pb)	$157.2^{-3.4}_{+3.8}$	$156.9^{-3.6}_{+1.8}$	$155.3^{-3.3}_{+3.3}$	$154.9^{-4.8}_{+2.9}$	$152.5^{-3.0}_{+4.5}$
$\sigma_{\rm RES}$(pb)	$154.3^{-1.1}_{+1.5}$	$154.0^{-1.2}_{+0.1}$	$152.4^{-1.0}_{+0.4}$	$152.0^{-2.4}_{+0.1}$	$150.0^{-0.7}_{+1.5}$

TABLE VII: The cross sections for t-channel single top production at LHC with $\sqrt{S}$=14 TeV, choosing transfer momentum cut $\sqrt{-\hat{t}} > 80$ GeV. The factorization scale uncertainties are also shown.

Acknowledgments

This work was supported in part by the National Natural Science Foundation of China, under Grants No. 10721063, No. 10975004 and No. 10635030.

m_t(GeV)	171	172	173	174	175
$\sigma_{\rm LO}$(pb)	$23.9^{-1.7}_{+1.2}$	$23.6^{-1.6}_{+1.1}$	$23.4^{-1.6}_{+1.1}$	$23.1^{-1.6}_{+1.1}$	$22.9^{-1.6}_{+1.1}$
$\sigma_{\rm NLO}$(pb)	$22.7^{-0.3}_{+0.8}$	$22.6^{-0.6}_{+0.4}$	$22.4^{-0.5}_{+0.4}$	$22.1^{-0.5}_{+0.5}$	$21.9^{-0.4}_{+0.6}$
$\sigma_{\rm RES}$(pb)	$22.3^{-0.1}_{+0.5}$	$22.2^{-0.4}_{+0.1}$	$22.1^{-0.2}_{+0.1}$	$21.8^{-0.2}_{+0.2}$	$21.5^{-0.1}_{+0.3}$

TABLE VIII: The cross sections for t-channel single antitop production at LHC with $\sqrt{S}$=7 TeV, choosing transfer momentum cut $\sqrt{-\hat{t}} > 80$ GeV. The factorization scale uncertainties are also shown.

m_t(GeV)	171	172	173	174	175
$\sigma_{\rm LO}$(pb)	$52.5^{-4.5}_{+3.4}$	$52.0^{-4.5}_{+3.4}$	$51.5^{-4.4}_{+3.3}$	$51.0^{-4.4}_{+3.3}$	$50.5^{-4.3}_{+3.3}$
$\sigma_{\rm NLO}$(pb)	$49.6^{-1.0}_{+1.2}$	$49.2^{-1.3}_{+0.9}$	$48.7^{-1.1}_{+1.1}$	$48.2^{-0.9}_{+1.2}$	$47.8^{-1.1}_{+1.1}$
$\sigma_{\rm RES}$(pb)	$48.9^{-0.4}_{+0.4}$	$48.5^{-0.7}_{+0.2}$	$48.0^{-0.5}_{+0.4}$	$47.5^{-0.3}_{+0.5}$	$47.1^{-0.5}_{+0.4}$

TABLE IX: The cross sections for t-channel single antitop production at LHC with $\sqrt{S}$=10 TeV, choosing transfer momentum cut $\sqrt{-\hat{t}} > 80$ GeV. The factorization scale uncertainties are also shown.

m_t(GeV)	171	172	173	174	175
$\sigma_{\rm LO}$(pb)	$103.1^{-10.4}_{+8.3}$	$102.2^{-10.3}_{+8.2}$	$101.2^{-10.2}_{+8.1}$	$100.3^{-10.1}_{+8.0}$	$99.4^{-10.0}_{+7.9}$
$\sigma_{\rm NLO}$(pb)	$96.7^{-2.0}_{+1.9}$	$96.3^{-2.6}_{+1.4}$	$95.1^{-2.2}_{+1.8}$	$94.1^{-2.5}_{+2.1}$	$93.1^{-2.5}_{+1.8}$
$\sigma_{\rm RES}$(pb)	$95.4^{-0.9}_{+0.4}$	$95.0^{-1.4}_{+0.1}$	$93.8^{-1.0}_{+0.6}$	$92.8^{-1.3}_{+0.6}$	$91.8^{-1.4}_{+0.8}$

TABLE X: The cross sections for t-channel single antitop production at LHC with $\sqrt{S}$=14 TeV, choosing transfer momentum cut $\sqrt{-\hat{t}} > 80$ GeV. The factorization scale uncertainties are also shown.

Appendix A: Relevant anomalous dimensions and matching coefficients

The various anomalous dimensions needed in our calculations can be found, e.g., in [25, 28, 30]. We list them below for convenience of the reader. The QCD β function is

$$\beta(\alpha_s) = -2\alpha_s \left[\beta_0 \frac{\alpha_s}{4\pi} + \beta_1 \left(\frac{\alpha_s}{4\pi}\right)^2 + \cdots\right], \tag{A1}$$

	NLO[8–10]	Res.[15–17]	Res.in SCET	Experiments.[29]
s-channel	0.99 pb	1.12 pb	1.04 pb	—
t-channel	2.15 pb	2.34 pb	2.04 pb	—
combined s- and t-channel	3.14 pb	3.46 pb	3.08 pb	2.76 pb

TABLE XI: Combination of s- and t-channel single top production at the Tevatron with $\sqrt{S}$=1.96 TeV.

with expansion coefficients

$$\begin{aligned}
\beta_0 &= \frac{11}{3}C_A - \frac{4}{3}T_F n_f, \\
\beta_1 &= \frac{34}{3}C_A^2 - \frac{20}{3}C_A T_F n_f - 4C_F T_F n_f, \\
\beta_2 &= \frac{2857}{54}C_A^3 + \left(2C_F^2 - \frac{205}{9}C_F C_A - \frac{1415}{27}C_A^2\right) T_F n_f + \left(\frac{44}{9}C_F + \frac{158}{27}C_A\right) T_F^2 n_f^2, \quad \text{(A2)}
\end{aligned}$$

where $C_A = 3$, $T_F = 1/2$ for QCD, and n_f is the number of active quark flavor.

The cusp anomalous dimension is

$$\Gamma_{\text{cusp}}(\alpha_s) = \Gamma_0 \frac{\alpha_s}{4\pi} + \Gamma_1 \left(\frac{\alpha_s}{4\pi}\right)^2 + \cdots\,, \quad \text{(A3)}$$

with

$$\begin{aligned}
\Gamma_0 &= 4C_F, \\
\Gamma_1 &= 4C_F \left[\left(\frac{67}{9} - \frac{\pi^2}{3}\right) C_A - \frac{20}{9}T_F n_f\right], \\
\Gamma_2 &= 4C_F \left[C_A^2 \left(\frac{245}{6} - \frac{134}{27}\pi^2 + \frac{11}{45}\pi^4 + \frac{22}{3}\zeta_3\right) + C_A T_F n_f \left(-\frac{418}{27} + \frac{40}{27}\pi^2 - \frac{56}{3}\zeta_3\right) \right. \\
&\quad \left. + C_F T_F n_f \left(-\frac{55}{3} + 16\zeta_3\right) - \frac{16}{27}T_F^2 n_f^2\right]. \quad \text{(A4)}
\end{aligned}$$

The other anomalous dimensions are expanded as eq. (A3), and their expansion coefficients are

$$
\begin{aligned}
\gamma_q^0 &= -3C_F, \\
\gamma_q^1 &= C_F^2\left(-\frac{3}{2}+2\pi^2-24\zeta_3\right)+C_FC_A\left(-\frac{961}{54}-\frac{11}{6}\pi^2+26\zeta_3\right)+C_FT_Fn_f\left(\frac{130}{27}+\frac{2}{3}\pi^2\right), \\
\gamma_Q^0 &= -2C_F, \\
\gamma_Q^1 &= C_FC_A\left(\frac{2}{3}\pi^2-\frac{98}{9}-4\zeta_3\right)+\frac{40}{9}C_FT_Fn_f, \\
\gamma_\phi^0 &= 3C_F, \\
\gamma_\phi^1 &= C_F^2\left(\frac{3}{2}-2\pi^2+24\zeta_3\right)+C_FC_A\left(\frac{17}{6}+\frac{22}{9}\pi^2-12\zeta_3\right)-C_FT_Fn_f\left(\frac{2}{3}+\frac{8}{9}\pi^2\right), \\
\gamma_j^0 &= -3C_F, \\
\gamma_j^1 &= C_F^2\left(-\frac{3}{2}+2\pi^2-24\zeta_3\right)+C_FC_A\left(-\frac{1769}{54}-\frac{11}{9}\pi^2+40\zeta_3\right) \\
&\quad +C_FT_Fn_f\left(\frac{242}{27}+\frac{4}{9}\pi^2\right). \qquad \text{(A5)}
\end{aligned}
$$

γ_{up}^V, γ_{dn}^V and γ^S can be obtained from the anomalous dimensions above through the following equations:

$$
\begin{aligned}
\gamma_{up}^V &= 2\gamma_q, \\
\gamma_{dn}^V &= \gamma_q+\gamma_Q, \\
\gamma^S &= -2\gamma_\phi-\gamma_h+\gamma_j. \qquad \text{(A6)}
\end{aligned}
$$

Appendix B: Calculation of the soft functions

In this appendix, we present the details of the calculation of the two $\mathcal{O}(\alpha_s)$ soft functions $S_{bt}^{(1)}(k,\mu)$ and $S_{tt}^{(1)}(k,\mu)$. We choose to do the calculation in the rest frame of top quark, in which the four-velocity of the top quark is $v^\mu=(1,0,0,0)$. This choice of the frame makes the denominators simple but leave the complexity in the delta functions. Actually, we also perform the calculation in the frame where the delta functions is simple but the singularities in the denominators are hard to isolate [31]. And finally we obtain the same results, which can be considered as a cross check for our calculations.

In the rest frame of top quark, we choose $n_b^\mu=(1,0,0,1)$. Then,

$$
q^\mu = q^+\frac{\bar{n}_b^\mu}{n_{b\bar{b}}}+q^-\frac{n_b^\mu}{n_{b\bar{b}}}+q_\perp^\mu, \quad n_1^\mu = n_1^+\frac{\bar{n}_b^\mu}{n_{b\bar{b}}}+n_1^-\frac{n_b^\mu}{n_{b\bar{b}}}+n_{1\perp}^\mu, \qquad \text{(B1)}
$$

and

$$q\cdot n_1 = \frac{q^+ n_1^- + q^- n_1^+}{n_{b\bar{b}}} - |q_\perp||n_{1\perp}|\cos\theta, \quad q\cdot v = q\cdot\frac{(n_b+n_{\bar{b}})}{2} = \frac{(q^+ + q^-)}{2}. \tag{B2}$$

Substituting these expressions into eq. (24), we get

$$\begin{aligned} S_{bt}^{(1)}(k,\mu) \;=\; & \frac{g_s^2 C_F \mu^{2\epsilon}}{(2\pi)^{d-1}} \int_0^\infty \mathrm{d}q^+ \int_0^\infty \mathrm{d}q^- \int \mathrm{d}\Omega_{d-2} \left(\frac{2q^+q^-}{n_{b\bar{b}}}\right)^{-\epsilon} \\ & \delta(k - \frac{q^+ n_1^- + q^- n_1^+}{n_{b\bar{b}}} + |q_\perp||n_{1\perp}|\cos\theta)\frac{n_b\cdot v}{q^+(q^+ + q^-)}. \end{aligned} \tag{B3}$$

Now redefine the integration variables q^+ and q^- and define $a = \frac{n_1^+}{n_1^-}$, then

$$\begin{aligned} S_{bt}^{(1)}(k,\mu) \;=\; & \frac{g_s^2 C_F \mu^{2\epsilon}}{(2\pi)^{d-1}} \int_0^\infty \mathrm{d}q^+ \int_0^\infty \mathrm{d}q^- \int \mathrm{d}\Omega_{d-2} \left(\frac{2n_{b\bar{b}}}{n_1^+ n_1^-}\right)^{-\epsilon} \\ & \delta(k - q^+ - q^- + 2\sqrt{q^+q^-}\cos\theta)\frac{n_b\cdot v}{q^+(aq^+ + q^-)}. \end{aligned} \tag{B4}$$

Introducing two variables x and y such that $q^+ = kyx$ and $q^- = ky(1-x) = ky\bar{x}$,

$$\begin{aligned} S_{bt}^{(1)}(k,\mu) \;=\; & \frac{g_s^2 C_F \mu^{2\epsilon}}{(2\pi)^{d-1}} \left(\frac{2n_{b\bar{b}}}{n_1^+ n_1^-}\right)^{-\epsilon} k^{-1-2\epsilon} \int \mathrm{d}\Omega_{d-2} \int_0^1 \mathrm{d}x \\ & x^{-1-\epsilon}\frac{(1-2\sqrt{x\bar{x}}\cos\theta)^{2\epsilon}\bar{x}^{-\epsilon}}{ax+\bar{x}}. \end{aligned} \tag{B5}$$

The singularity in the integrand can be isolated by

$$x^{-1-\epsilon} = -\frac{1}{\epsilon}\delta(x) + \left(\frac{1}{x}\right)_+ - \epsilon\left(\frac{\ln x}{x}\right)_+ + \mathcal{O}(\epsilon^2). \tag{B6}$$

Completing the above three parts of the integration separately and expanding

$$\frac{1}{k^+}\left(\frac{\tilde{\mu}}{k^+}\right)^{2\epsilon} = -\frac{1}{2\epsilon}\delta(k^+) + \left[\frac{1}{k^+}\right]_\star^{[k^+,\tilde{\mu}]} - 2\epsilon\left[\frac{1}{k^+}\ln\frac{k^+}{\tilde{\mu}}\right]_\star^{[k^+,\tilde{\mu}]} + \mathcal{O}(\epsilon^2), \tag{B7}$$

we get

$$S_{bt}^{(1)}(k,\mu) \;=\; \tfrac{2C_F\alpha_s}{4\pi}\left\{4\left[\frac{\ln\frac{k}{\tilde{\mu}}}{k}\right]_\star^{[k,\tilde{\mu}]} + \delta(k)c_{bt}^S\right\}, \tag{B8}$$

where $c_{bt}^S = -\ln^2(1+\frac{1}{a}) - 2\mathrm{Li}_2(\frac{1}{1+a}) + \frac{\pi^2}{12}$.

In a similar but simpler way, we can get $c_{tt}^S = -4\ln(1+\frac{1}{a})$.

---

[1] Tevatron Electroweak Working Group and CDF and D0, [arXiv:0903.2503[hep-ex]]

[2] C. Amsler et al., Phys. Lett. B **667** (2008) 1

[3] Bernreuther and Werner, Phys. Lett. B **667** (2008) 1

[4] V.M. Abazov et al. [D0 Collaboration], Phys. Rev. Lett **103** (2009) 092001 [arXiv:0903.0850[hep-ex]]

[5] T. Aaltonen et al. [CDF Collaboration], Phys. Rev. Lett **103** (2009) 092002 [arXiv:0903.0885[hep-ex]]

[6] G. Bordes and B. van Eijk, Nucl. Phys. **B 435** (1995) 23

[7] T. Stelzer and S. Willenbrock, Phys. Lett. **B 357** (1995) 125 [arXiv:hep-ph/9505433]

[8] B.W. Harris, E. Laenen, L. Phaj, Z, Sullivan and S. Weinzierl, Phys. Rev. **D 66** (2002) 054024 [arXiv:hep-ph/0207055]

[9] Z. Sullivan, Phys. Rev. **D 70** (2004) 114012 [arXiv:hep-ph/0408049]

[10] J.M. Compell, R.K. Ellis and F. Tramontano, Phys. Rev. **D 70** (2004) 094012 [arXiv:hep-ph/0408158]

[11] Q.-H. Cao and C.-P. Yuan, Phys. Rev. **D 71** (2005) 054022 [arXiv:hep-ph/0408180]

[12] Q.-H. Cao, R. Schwienhorst, J.A. Benitez, R. Brock and C.-P. Yuan, Phys. Rev. **D 72** (2005) 094027 [arXiv:hep-ph/0504230]

[13] S. Frixione, E. Laenen, P. Motylinski, and B.R. Webber, JHEP **03** (2006) 092 [arXiv:hep-ph/0512250]

[14] S. Alioli, P. Nason, C. Oleari and E. Re, JHEP **09** (2009) 111 [arXiv:0907.4076[hep-ph]]

[15] N. Kidonakis, Phys. Rev. **D 74** (2006) 114012 [arXiv:hep-ph/0609287]

[16] N. Kidonakis, Phys. Rev. **D 75** (2007) 071501 [arXiv:hep-ph/0701080]

[17] N. Kidonakis, Phys. Rev. **D 81** (2010) 054028 [arXiv:1001.5034[hep-ph]]

[18] C.W. Bauer, S. Fleming and M.E. Luke Phys. Rev. **D 63** (2000) 014006 [arXiv:hep-ph/0005275]

[19] C.W. Bauer, S. Fleming, D. Pirjol and I.W. Stewart Phys. Rev. **D 63** (2001) 114020 [arXiv:hep-ph/0011336]

[20] C.W. Bauer and I.W. Stewart Phys. Rev. **B 516** (2001) 134 [arXiv:hep-ph/0107001]

[21] C.W. Bauer, D. Pirjol and I.W. Stewart Phys. Rev. **D 65** (2002) 054022 [arXiv:hep-ph/0109045]

[22] T. Becher, and M. Neubert Phys. Rev. Lett. **97** (2006) 082001 [arXiv:hep-ph/0605050]

[23] H.X. Zhu, C.S. Li, J. Wang and J.J. Zhang, [arXiv:1006.0681]

[24] I.A. Korchemskaya and G.P. Korchemsky, Phys. Lett. **B 287** (1992) 169

[25] T. Becher, M. Neubert and B.D. Pecjak JHEP **01** (2007) 076 [arXiv:hep-ph/0607228]

[26] C.W. Bauer, A. Horig and F.J. Tackmann Phys. Rev. **D 79** (2009) 114013 [arXiv:0808.2191[hep-ph]]

[27] J. Chay, C. Kim, Y.G. Kim and J.-P. Lee Phys. Rev. **D 71** (2005) 056001 [arXiv:hep-ph/0412110]

[28] T. Becher and M.D. Schwartz, JHEP **02** (2010) 040 [arXiv:0911.0681[hep-ph]]

[29] Tevatron Electroweak Working Group and CDF and D0 Collaboration, [arXiv:0908.2171[hep-ex]]

[30] T. Becher M. Neubert and G. Xu, JHEP **07** (2008) 030 [arXiv:0710.0680[hep-ph]]

[31] R. Kelley and M.D. Schwartz [arXiv:1008.4355[hep-ph]]